

An Experimental Investigation on APR1400 Penetration Weld Failure by Metallic Melt

Sang Mo An^{a*}, Kwang Soon Ha^a, Hwan Yeol Kim^a

^aKorea Atomic Energy Research Institute, 989-111 Daedeok-daero, Yuseong-gu, Daejeon, Republic of Korea

*Corresponding author: sangmoan@kaeri.re.kr

1. Introduction

Korean PWRs (pressurized water reactors) have several ICI (in-core instrumentation) penetration tubes that penetrate the reactor vessel through the reactor bottom head. OPR1000 and APR1400 have 45 and 61 ICI penetrations to monitor the in-core status [1]. Most BWRs (boiling water reactors) have more than one hundred penetrations including the control rod, in-core guide tube, and drain nozzle at the reactor lower head [2]. The configuration of the ICI penetration tube at the center of APR1400 reactor bottom head is shown in Fig. 1. Even though the configurations and installation methodology of the penetrations vary from vendor design to design, they are attached to the inside of the reactor bottom head by a partial penetration weld as shown in Fig. 1. Therefore, the penetrations are considered as the most vulnerable parts with respect to the reactor vessel failure when a core melt severe accident occurs and the corium reaches the lower head.

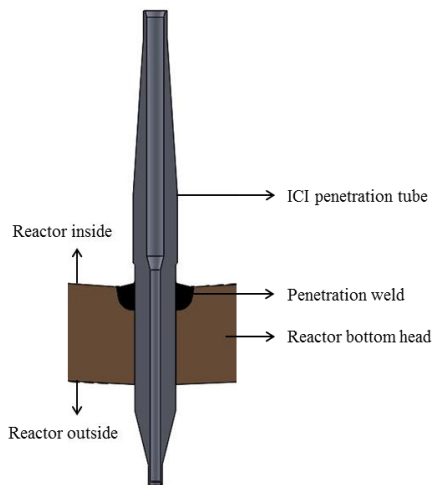


Fig. 1. Configuration of an ICI penetration tube in APR1400 reactor.

Penetration tube failure modes can be divided into two categories; tube ejection out of the vessel lower head and rupture of the penetration tube outside the vessel [2]. Tube ejection begins with degrading the penetration tube weld strength to zero as the weld is exposed to temperatures as high as the weld melting temperature, which is called weld failure, and then overcoming any binding force in the hole in the vessel wall that results from differential thermal expansion of the tube and vessel wall. Tube rupture assumes that the debris bed has melted the instrument tube inside the reactor and melt migrates down into the tube to a

location outside the vessel wall where a pressure rupture can occur, thus breaching the pressure boundary.

In the present paper, we have a focus on the tube ejection failure mode, specifically on the APR1400 weld failure by direct contact with a metallic melt. The objective is to investigate experimentally the ablation kinetics of an APR1400 penetration weld during the interactions with a metallic melt and to suggest the modification of the existing weld failure model. This paper involves the interaction experiments of two different metallic melts (metallic corium and stainless steel melts) with a weld specimen, and rough estimation of weld failure time.

2. Experimental Setup

Figure 2 shows an experimental facility, VESTA-S (Verification of Ex-vessel corium STAbilization-Small), to investigate the penetration weld ablation kinetics by an interaction with a metallic melt. The VESTA-S facility was introduced in a few papers [3, 4] and a detail description on the operation procedure and melt generation technique can be found in those papers. Two kinds of metallic melts were employed for the experiments: one is metallic corium melt composed of Fe 46%, U 31%, Zr 16%, and Cr 7% of the total mass, and the other is stainless steel (SUS304) melt. The stainless steel has an average composition of Fe 70%, Cr 19%, and Ni 11%.

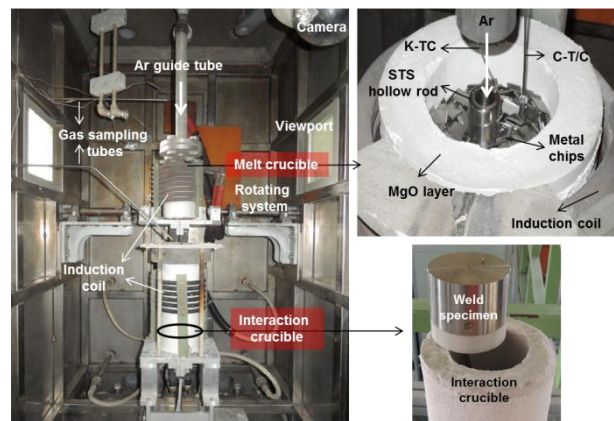


Fig. 2. Experimental setup.

Figure 3 shows the configurations of melt and interaction crucibles with a weld specimen. The crucibles consist of tube assembly which is cooled by water flowing into each tube. Magnesium oxide (MgO) layer is sintered on the inner wall of the crucible to protect the crucibles from the melt. The crucibles are surrounded by a water-cooled induction coil to supply

electro-magnetic energy for heating. A high-frequency power generator can supply electric power to the induction coil up to 225 kW with 76 Hz.

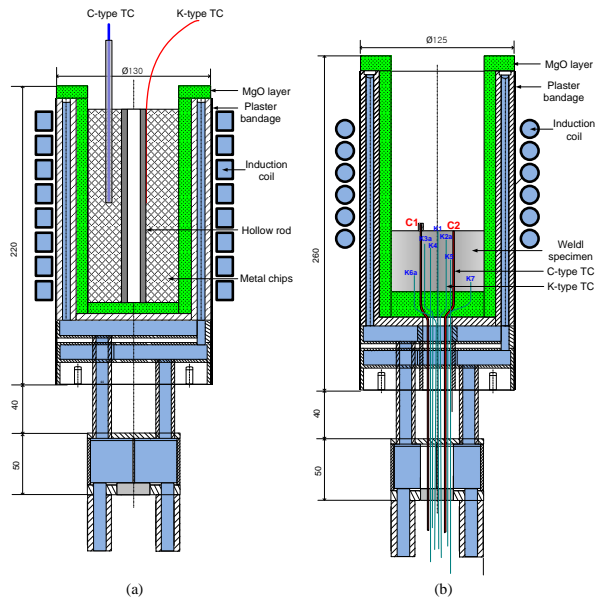


Fig. 3. Configuration of a cold crucible; (a) melt crucible, (b) interaction crucible.

A metallic melt is generated in a melt crucible, where nearly 3 kg of metallic melt can be generated. A C-type thermocouple (0-2320 °C, ±1% error) shielded by tungsten or alumina tubes and an optical pyrometer (Modline 3, IRCON, 1500-3500°C, ±0.6% error) were used to measure the melt temperature. During the whole experimental process, argon gas was purged into the test chamber through a guide tube installed between the top of the melt crucible and the optical pyrometer to create an inert atmosphere inside the chamber and secure the optical path by removing aerosols produced from the melt. A hollow rod was also installed at the center of the melt crucible to make rays emitted from the melt into blackbody radiation, and the rod temperature was monitored by a K-type thermocouple (-200-1370°C, ±1% error).

If the melt reaches a certain intended temperature (~2000°C), it is delivered down into the interaction crucible by a remote-controlled rotating system. A cylindrical shape of a weld specimen is located at the bottom of the interaction crucible. Once the melt is delivered, the weld specimen interacts with the delivered melt immediately, and the delivered melt is instantaneously heated up for sustained heating.

The weld specimens were supplied by Doosan Heavy Industries & Construction. The weld material is J-groove filter metal (ENiCrFe-7 UNS No. W86152), which is used for welding ICI penetration tubes (Inconel-690) at the APR1400 bottom head. The weld specimens were manufactured in accordance with the standard J-groove weld buildup process and then machined to have a 75 mm diameter and 50 mm thickness. As shown in Fig. 4, there are ten K-type thermocouples embedded inside the weld specimen for

measuring the temperature distributions, as well as two C-type thermocouples for measuring the delivered melt temperature. The K-type thermocouples are positioned to have different radii and depths, and accordingly to have different distances from the top center of the specimen surface ('K1' in Fig. 4). Therefore, the ablation rate can be evaluated by thermocouple readings during the melt-concrete interaction by assuming that the melt front maintains a hemispherical shape.

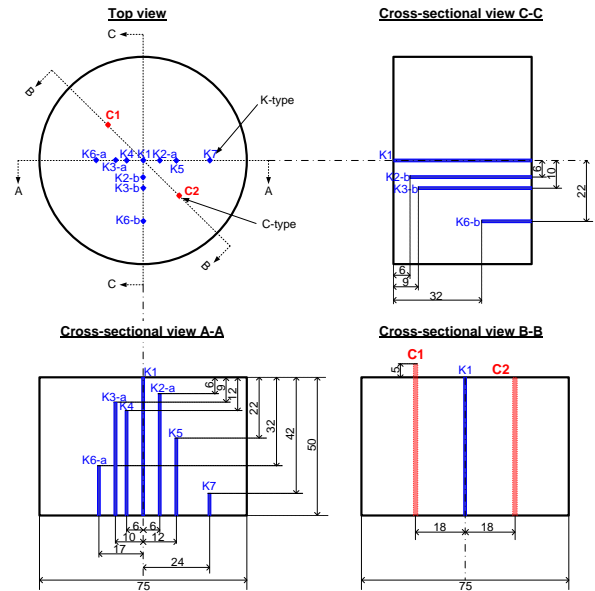


Fig. 4. Locations of thermocouples embedded inside the weld specimen.

3. Results and Discussion

3.1 Experimental Results

The experimental conditions and main results are summarized in Table I. Figures 5 and 6 show the temperature history during the melt generation for corium melt and stainless steel melt, respectively. The generator power was increased gradually for the stable melt generation. In the early heating stage, the K-type thermocouple readings of the hollow steel rod displayed similar increasing patterns as the C-type thermocouple readings of the melt. However, the K-type readings transmitted a meaningless signal owing to the failure since it reached the maximum measuring limit (~1400°C).

Table I: Summary of experimental conditions and results

Test ID	C1	S1
Melt	Metallic corium	Stainless steel
Charged metal mass (kg)	3.129	2.216
Delivered melt mass (kg)	1.756	1.751
Delivery rate (%)	56	79
Instant maximum melt temperature (°C)	1864	1890
Ablation rate (mm/s)	0.109	0.244

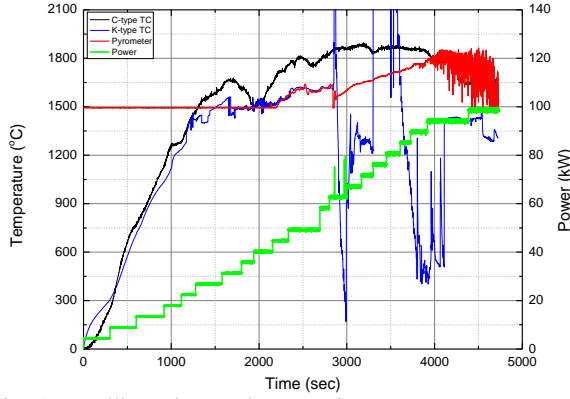


Fig. 5. Metallic corium melt generation process.

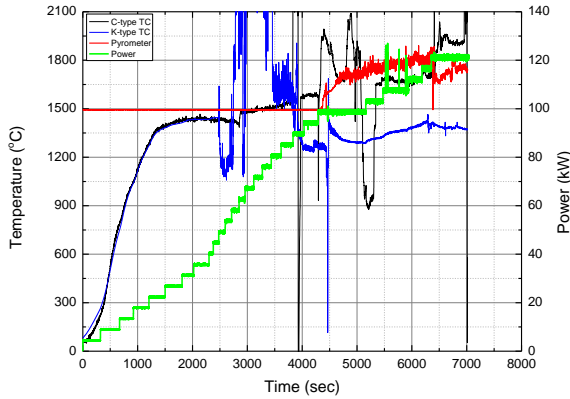


Fig. 6. Stainless steel melt generation process.

The pyrometer readings near the end of melt generation process showed larger fluctuations because more aerosols were generated in high melt temperature ranges, which obstructs the optical path of a pyrometer and makes it difficult to measure the real melt temperature.

Figures 7 and 8 show the thermocouple readings (see Fig. 4 for each location) during the melt-concrete interaction for the C1 and S1 tests, respectively. As shown in the figures, the thermocouple readings in case of the interaction with a relative high temperature of stainless steel melt showed more rapid increase than the interaction with metallic corium melt. The propagating speed of the interaction front into the weld specimen (i.e., ablation rate) was quantified under the assumption that the interaction front reaches the thermocouple at the

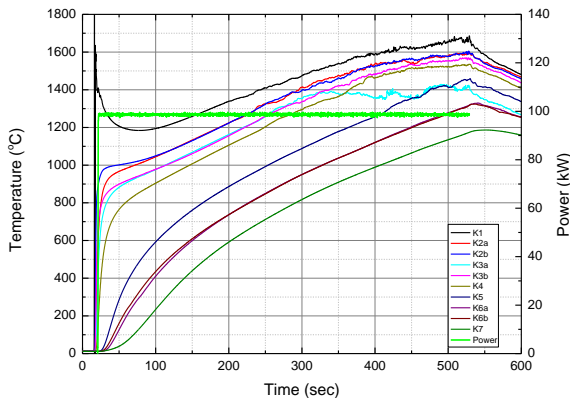


Fig. 7. Thermocouple readings embedded in the weld specimen during the interaction with metallic corium melt.

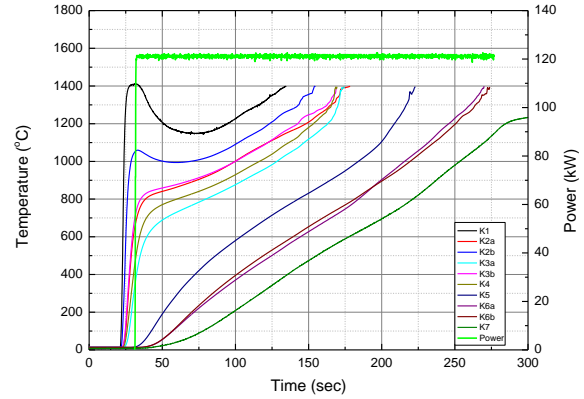


Fig. 8. Thermocouple readings embedded in the weld specimen during the interaction with stainless steel melt.

instant time when its temperature increases suddenly up to 1200°C. The ablation rate values are listed in Table I.

3.2 Weld Failure Model

The weld failure criterion is given as [2, 5]

$$\sigma_u \leq \sigma_e, \quad (1)$$

where σ_u is the ultimate strength of the weld, and the effective stress σ_e is expressed as

$$\sigma_e = \sqrt{3}\tau_w = \sqrt{3}\left(\frac{p_i r_o}{2L_w}\right), \quad (2)$$

where τ_w is the shear stress in the weld; p_i , pressure inside the reactor vessel; r_o , tube outer radius; L_w , weld length. In the weld failure model above, the ablation of weld length was not considered, that is, L_w has a certain fixed value. However, as described in the experiments, the weld length could be reduced due to the weld ablation by high temperature melt. In that case, Eq. (2) needs to be modified considering the weld ablation rate as follows:

$$\sigma_e = \sqrt{3}\tau_w = \sqrt{3}\left(\frac{p_i r_o}{2[L_o - (W_{\text{weld}} \times t)]}\right), \quad (3)$$

where L_o is the initial weld length; W_{weld} , weld ablation rate; t , time. Equation (3) gives more conservative weld failure estimation than Eq. (2) because the weld length decreases with time and thus the effective stress imposed on the weld increases. The vertical weld length in APR1400 penetration is about 43 mm, which implies that the weld length becomes zero within the time range from 176 seconds ($W_{\text{weld}} = 0.109$ mm/s for metallic corium melt) to 394 seconds ($W_{\text{weld}} = 0.244$ mm/s for

stainless steel melt) after the interaction with the melt. However, the exact weld failure time depends on the melt compositions and temperatures according to the severe accident scenarios. Therefore, it is recommended to the readers to refer to the order of weld ablation rate and weld failure time.

3. Conclusions

The interaction experiments between the metallic melts and an APR1400 penetration weld were performed to investigate the ablation kinetics of the penetration weld. Metallic corium and stainless steel melts were generated using an induction heating technique and interacted with a penetration weld specimen. The ablation rate of the weld specimen showed a range from 0.109 to 0.244 mm/s and thus the APR1400 penetration weld was estimated to be failed at hundreds of times after the interaction with the melt. Moreover, we suggested a necessity to modify the existing weld failure criterion considering the weld ablation rate. For reasonable estimation of the weld ablation rate and subsequent tube ejection failure time, we need more experimental data with various melt compositions and temperatures, which left as a future work.

ACKNOWLEDGMENTS

This work was supported by the National Research Foundation of Korea (NRF) grant funded by the Korea government (MEST) (No. 2012M2A8A4025885). The authors gratefully acknowledged Doosan Heavy Industries & Construction's support in the provision of Inconel-690 weld material.

REFERENCES

- [1] S. M. An and H. Y. Kim, Revisit of Penetration Failure Models and Calculations for APR1400 ICI Penetrations, Proceedings of Korean Nuclear Society Autumn Meeting, Gyeongju, Korea, Oct. 24-25, 2013.
- [2] J. L. Rempe, S. A. Chavez, G. L. Thinner, G. M. Allison, G. E. Korth, R. J. Witt, J. J. Sienicki, S. K. Wang, L. A. Stickler, C. H. Heath and S. D. Snow, Light Water Reactor Lower Head Failure Analysis, NUREG/CR-5642, 1993.
- [3] K. S. Ha, S. M. An, B. T. Min and H. Y. Kim, Cold Crucible Technique for Interaction Test of Molten Corium with Structure, Proceedings of Korean Nuclear Society Autumn Meeting, Gyeongju, Korea, Oct. 25-26, 2012.
- [4] S. M. An, K. S. Ha, B. T. Min, S. H. Hong and H. Y. Kim, Experimental Study on the Molten Corium Interaction with Structure by Induction Heating Technique, Proceedings of Korean Nuclear Society Spring Meeting, Jeju, Korea, May 29-30, 2014.
- [5] MAAP5 Code Manual, Fauske & Associates, Inc, 2008.